Univerzita Karlova v Praze
Matematicko-fyzikální fakulta

BAKALÁŘSKÁ PRÁCE

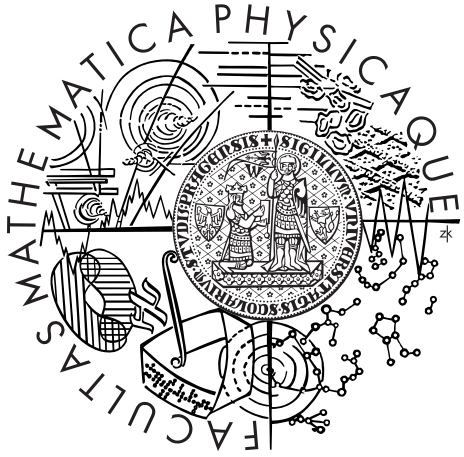

Jan Moudřík

Studium magnetismu ve sloučeninách $CeTX_3$

Katedra fyziky kondenzovaných látek

Vedoucí bakalářské práce: RNDr. Jan Prokleška, Ph.D.
Studijní program: Fyzika (B1701)
Studijní obor: FOF (1701R026)

Praha 2013

Charles University in Prague
Faculty of Mathematics and Physics

BACHELOR THESIS

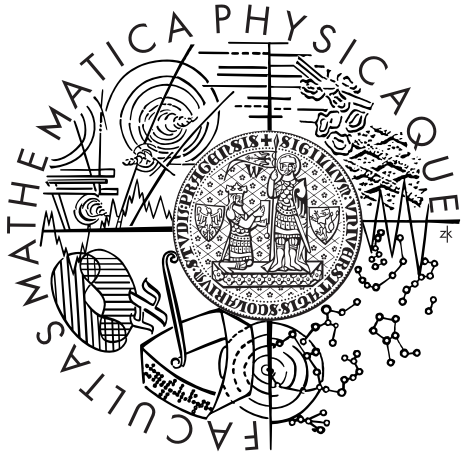

Jan Moudřík

Study of magnetic behaviour in $CeTX_3$ compounds

Department of Condensed Matter Physics

Supervisor of the bachelor thesis: RNDr. Jan Prokleška, Ph.D.

Study programme: Fyzika (B1701)

Specialization: FOF (1701R026)

Prague 2013

Foremostly, I would like to thank RNDr. Jan Prokleška, Ph.D. for his kind and patient support. I would also like to thank prof. RNDr. Vladimír Sechovský, DrSc. and Ao. Univ. Prof. Dr. Herwig Michor for giving me the opportunity to have such a beneficial experience of working at the Department of Condensed Matter Physics of Charles University in Prague and at the Institute of Solid State Physics at Vienna University of Technology. Last but not least, I want to thank Josef Moudřík for proofreading and my whole family for their tireless love and support.

I declare that I carried out this bachelor thesis independently, and only with the cited sources, literature and other professional sources.

I understand that my work relates to the rights and obligations under the Act No. 121/2000 Coll., the Copyright Act, as amended, in particular the fact that the Charles University in Prague has the right to conclude a license agreement on the use of this work as a school work pursuant to Section 60 paragraph 1 of the Copyright Act.

In ..... date ..... signature of the author

Název práce: Studium magnetismu ve sloučeninách $CeTX_3$

Autor: Jan Moudřík

Katedra: Katedra fyziky kondenzovaných látek

Vedoucí bakalářské práce: RNDr. Jan Prokleška, Ph.D.

Abstrakt: Studovali jsme tuhé roztoky $CeTX_3$ sloučenin (T a X značí tranzitivní kovy a Si/Ge) s $BaNiSn_3$ strukturou. Úspěšně jsme připravili polykrystalické vzorky $CeCo_xRh_{1-x}Si_3$ ($x = 0,5$, $x = 0,8$, $x = 0,9$ a $x = 1,0$) a $CeIr(Si_xGe_{1-x})_3$ ($x = 0,1$, $x = 0,4$, $x = 0,6$ a $x = 0,8$). Všechny 4 vzorky $CeCo_xRh_{1-x}Si_3$ přešly do supravodivého stavu při teplotě 0,7–0,9 K. Na základě výsledků měření tepelné kapacity jsme došli k závěru, že supravodivost je pravděpodobně způsobena příměsí. Určili jsme krystalografické, termodynamické a magnetické vlastnosti tuhého roztoku $CeIr(Si_xGe_{1-x})_3$ včetně teploty přechodu do magneticky uspořádaného stavu. Teplota těchto přechodů se ve vzorcích s různou substitucí příliš neměnila, na rozdíl od charakteru přechodů, který se měnil značně.

Klíčová slova: magnetismus, nízké teploty, substituce

Title: Study of magnetic behaviour in $CeTX_3$ compounds

Author: Jan Moudřík

Department: Department of Condensed Matter Physics

Supervisor: RNDr. Jan Prokleška, Ph.D.

Abstract: Solid solutions of $BaNiSn_3$ type $CeTX_3$ (T and X denote a transition metal and Si/Ge, respectively) compounds were studied. Polycrystalline samples of solid solutions $CeCo_xRh_{1-x}Si_3$ ($x = 0.5$, $x = 0.8$, $x = 0.9$ and $x = 1.0$) and $CeIr(Si_xGe_{1-x})_3$ ($x = 0.1$, $x = 0.4$, $x = 0.6$ and $x = 0.8$) were successfully grown. A superconducting transition at 0.7–0.9 K was exhibited by all four compositions of the solution $CeCo_xRh_{1-x}Si_3$. Based on measurements of specific heat, we conclude that the superconductivity is probably caused by impurity phases. We have determined crystallographic, thermodynamic and magnetic properties of the solution $CeIr(Si_xGe_{1-x})_3$. Magnetic phase transition temperatures were established, the character of the transitions changed significantly in all four compositions, the temperatures themselves did not.

Keywords: magnetism, low temperature, substitution

Contents

Introduction

As most of $CeTX_3$ compounds (T and X denote a transition metal and Si/Ge, respectively), $CeCoSi_3$, $CeRhSi_3$, $CeIrSi_3$ and $CeIrGe_3$ crystallize in the $BaNiSn_3$ type tetragonal structure with the space group I4mm (No.107). The point group of the $BaNiSn_3$ type structure is C_{4v}, which lacks the mirror plane and a two-fold axis normal to the c axis (z axis) [1]. This type of structure also lacks an inversion centre which makes the whole group quite interesting since $CeRhSi_3$ [2], $CeIrSi_3$ [3] and $CeIrGe_3$ [4] are pressure-induced superconductors. The compound $CeCoSi_3$ was conflictingly reported to show a superconducting transition at 0.7–1.2 K [5] but also no superconductivity down to 0.5 K [6]. Figure 1 displays the $BaNiSn_3$ type crystal lattice.

$CeCoSi_3$ does not order magnetically down to 0.5 K [6] but $CeRhSi_3$ is an antiferromagnet and orders at 1.8 K [7]. $CeIrSi_3$ is an antiferromagnetic metal which orders at 5 K whereas $CeIrGe_3$ shows three magnetic transitions – an antiferromagnetic transition at 8.7 K and two unknown transition at 4.7 K and 0.7 K [7]. Magnetization measurements carried out in Ref. [8] indicate that the compound below 4.7 K is ferromagnetic with a small magnetic moment of 0.14 μ_B/Ce at 2 K. The compound $CeIrGe_3$ obeys the Curie-Weiss law above about 100 K with a negative Weiss temperature Θ = -21 K and has an effective magnetic moment of 2.39 μ_B whereas the compound $CeIrSi_3$ obeys the Curie-Weiss law above about 150 K with a very large negative Weiss temperature Θ = -142 K and has an effective magnetic moment of 2.62 μ_B [7].

The substitutions we are carrying out in the solid solutions $CeCo_xRh_{1-x}Si_3$ and $CeIr(Si_xGe_{1-x})_3$ can be viewed as an application of a negative chemical pressure. The idea of applying negative chemical pressure stems from the fact that the Ge (Rh) cations have bigger radii than the Si (Co) ones. Therefore, the substitution of Ge (Rh) on Si-site (Co-site) is expected to linearly modify the lattice volume. Change of magnetic properties with respect to the substitution can be associated with the change of the lattice volume in a similar way as external pressure.

Figure 2 shows the Néel temperature T_N as a function of the unit-cell volume for $CeTX_3$ in which T belongs to the group 9 (Co, Rh and Ir) in the periodic table. The Néel temperature as a function of the unit cell volume peaks at approximately 186 Å^3.

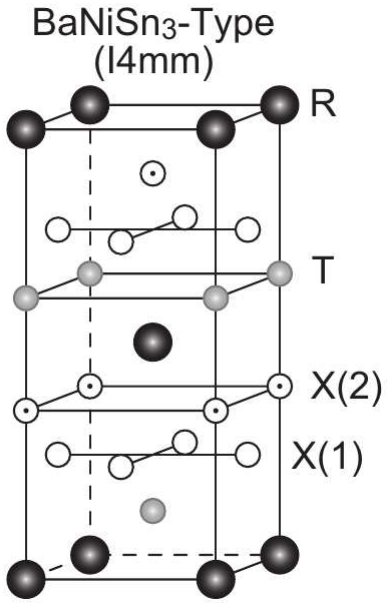

Figure 1: Tetragonal structure of $CeCoSi_3$, $CeRhSi_3$, $CeIrSi_3$ and $CeIrGe_3$, reprinted from Ref. [1].

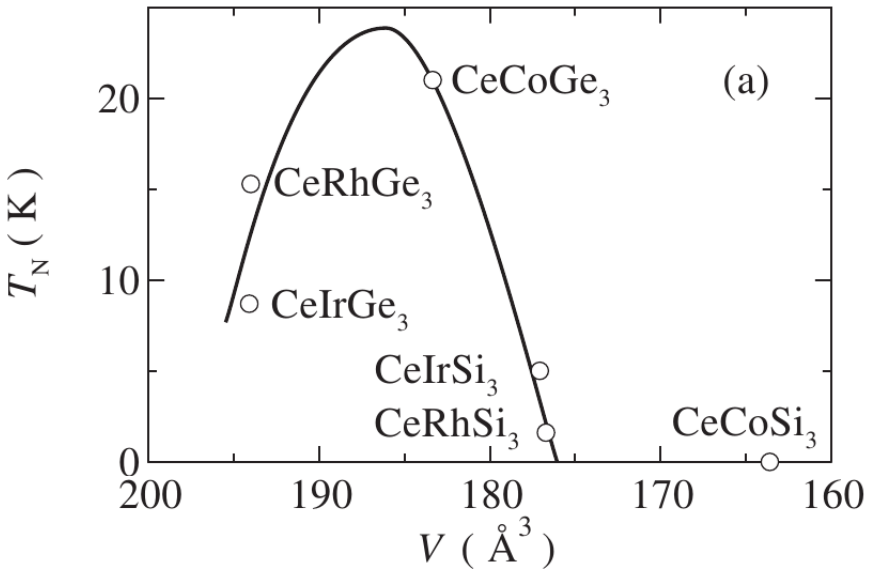

Figure 2: Unit cell volume dependence of the Néel temperature in $CeTSi_3$ and $CeTGe_3$ (T: Co, Rh, Ir), reprinted from Ref. [8].

1. Theory

1.1 X-ray Diffraction

The X-ray diffraction is one of the most common methods used for determination of a structure of crystalline materials. It is based on a constructive interference of X-rays which were specularly diffracted by the ions of the studied material. The X-rays are particularly suitable for this purpose since their wavelength is of the order of 1 Å, i.e. of the order of typical interatomic distances in a solid [9]. The condition for such interference is expressed in the Bragg law [10, formula 2.1]

$$2d \sin(\theta) = n\lambda, \tag{1.1}$$

where d is a spacing between parallel lattice planes, θ is the angle of incidence, n is a integral number and λ is the wavelength of the diffracted rays.

1.2 Heat capacity

If a homogeneous system absorbs a small amount of heat ΔQ causing its temperature to rise by ΔT then its heat capacity C is defined as

$$C = \frac{\Delta Q}{\Delta T}. \tag{1.2}$$

Specific heat is a heat capacity per unit mass or per mole. The change in entropy can be calculated using the specific heat (under the assumption that no work is being carried out) as

$$\Delta S = \int \frac{C(T)}{T}\,\mathrm{d}T. \tag{1.3}$$

The quantity

$$l = T\Delta s \tag{1.4}$$

is then called the specific latent heat of a transition [11] where Δs denotes a change in entropy per unit mass. When considering a phase transition from solid to liquid phase, for example, the latent heat of the transition is the quantity of heat required to melt one unit mass of solid.

Ehrenfest defines the order of a phase transition using the derivatives of the Gibbs potential per unit mass g_i of the two phases. The transition is of nth-order if at the transition point [11]

$$\frac{\partial^n g_1}{\partial T^n} \neq \frac{\partial^n g_2}{\partial T^n} \qquad \text{and} \qquad \frac{\partial^n g_1}{\partial P^n} \neq \frac{\partial^n g_2}{\partial P^n} \tag{1.5}$$

whereas all lower derivatives are equal.

Since entropy is related to the first derivative of Gibbs potential g using the equation 1.3 we see that the specific heat is related to the 2nd derivative of g. During the first order phase transition we therefore observe a change in entropy and according to equation 1.4 a latent heat is absorbed/released. During a second order phase transition on the other hand, the second derivatives of Gibbs potential are not continous and thus neither is the specific heat. A well-known example of a second-order transition is a transition to a superconducting state.

1.3 Superconductivity

Superconducting state is a state in which a material has zero electrical resistivity. Superconductivity occurs under a critical temperature T_c, under a critical field H_c and under a critical current density J_c. These critical conditions are not independent, meaning that for example the critical field of a specimen depends on the temperature of the specimen.

At the critical temperature the material undergoes a phase transition. In zero magnetic field the transition is observed to be of a second order, there is thus no latent heat involved. Since the superconducting state is more ordered than the normal state a decrease in entropy is observed and the transition is therefore evident as a discontinuity in the heat capacity [10]. As the temperature drops below T_c the specific heat jumps to a higher value and then slowly decreases, eventually falling well below the value one would expect for a normal metal [9].

1.4 Magnetic ordering

A magnetic moment of a free atom has three principal sources: the spin with which electrons are endowed; their orbital angular momentum; and the change in the orbital moment induced by an applied magnetic field [10]. Lets assume a solid to constitute of a large number of atoms each having a individual magnetic moment and a magnetization of such solid then to be the averaged vector sum of those moments. If there were no magnetic interactions in a zero magnetic field such solid would not exhibit any magnetization whatsoever, see [9, formula 31.44]. However, certain solids below critical temperatures display a spontaneous magnetization, i.e. a non-zero magnetization even in zero magnetic fields, and these are called magnetically ordered solids.

A basic magnetically ordered state of a solid is a ferromagnetic order in which the solid exhibits a spotaneous magnetic moment below the critical *Curie temperature* T_C. Paramagnetic susceptibility is given by the Curie law $\chi_p = C/T$, where C is the Curie constant. In the mean-field approximation it is assumed that each magnetic atom experiences apart from the applied magnetic field another field B_E, called the exchange field, which is proportional to the magnetization $B_E = \lambda M$ [10]. If we assume that a ferromagnet is a paramagnet with the additional magnetization caused by the exchange field we can derive an expression for a magnetic susceptibility χ of a ferromagnet in the paramagnetic region above the Curie point – the Curie-Weiss law [10, formula 12.4]

$$\chi = \frac{C}{T - T_C}. \tag{1.6}$$

Increasing the temperature and therefore increasing the entropy of the system causes eventually a breaking of the magnetic order and a transition to a paramagnetic state. The usual transition from ferromagnetic to paramagnetic state is of second order [10].

Another ordered magnetic state relevant to this study is a antiferromagnetic state in which the vector sum of the local magnetic moments averages to zero. A antiferromagnet thus does not exhibit a spotaneous magnetization even though the local magnetic moments display a certain ordering. A simple ilustration of

such mechanism is a case when all local magnetic moments are of the same absolute value but neighboring moments point in quite the opposite direction – such system is obviously ordered but the sum of all the moments over the whole macroscopic sample of such solid is zero. The critical temperature above which this ordering is no longer present is called the *Néel temperature* T_{N}.

Above the Néel temperature an antiferromagnet obeys the Curie-Weiss law in the form [10, figure 12.20]

$$\chi = \frac{C}{T - \Theta} + \chi_0 \tag{1.7}$$

where Θ denotes the Weiss temperature – it has the same meaning as the Curie temperature for ferromagnet, it is only of negative value – and χ_0 denotes the Pauli susceptibility. From the Curie-Weiss constant C one can calculate the effective magnetic moment μ_{eff} which expresses the number of effective Bohr magnetons using the relation [10, formula 11.22]

$$C = \frac{N\mu_{\mathrm{B}}^2\mu_{\mathrm{eff}}^2}{3k_{\mathrm{B}}}. \tag{1.8}$$

Since $[C] = \mathrm{emu/mol}$ the relation for the effective magnetic moment

$$\mu_{\mathrm{eff}} = \sqrt{\frac{3Ck_{\mathrm{B}}}{N_{\mathrm{A}}\mu_{\mathrm{B}}^2}}. \tag{1.9}$$

2. Sample Preparation and Characterization

2.1 Preparation

The samples of the solid solutions $CeIr(Si_xGe_{1-x})_3$ and $CeCo_xRh_{1-x}Si_3$ were prepared at the Technology Lab of Department of Condensed Matter Physics of Charles University [12].

Firstly, stoichiometric quantities of pure metals of Ce, Ir, Co, Rh, Si and Ge with respect to the desired compositions of $x = 0.5$, $x = 0.8$, $x = 0.9$ and $x = 1.0$ for $CeCo_xRh_{1-x}Si_3$ and $x = 0.1$, $x = 0.4$, $x = 0.6$ and $x = 0.8$ for $CeIr(Si_xGe_{1-x})_3$ were prepared. The desired polycrystal ingots were melted using an arc furnace, wrapped in a tantalum foil and sealed in a glass tube under protective atmosphere (Ar). Tantalum is very suitable for this purpose since it has the melting point at 3293 K [10, p. 51]. Polycrystals of masses of approximately 4 g were afterwards annealed using an electric furnace.

Using a diamond circular and a wire saw the samples were afterwards cut into pieces of appropriate size suitable for the measurements of heat capacity, electrical resistivity and magnetic susceptibility.

2.2 X-ray Diffraction

A part of the prepared samples was used for powder X-ray diffraction measurements. These were carried out at the Department of Condensed Matter Physics of Charles University in Prague using the powder diffractometer Bruker D8 Advance [13]. The powder diffractometer consists of a vertical goniometer, an X-ray tube with a copper anode and a energy dispersive X-ray detector. Rietveld refinements were carried out on the diffraction data using the FullProf program package [14].

2.3 Heat Capacity

Heat capacity of the solid solution $CeIr(Si_xGe_{1-x})_3$ was measured at the Institute of Solid State Physics at Vienna University of Technology [15] using the adiabatic heat-pulse calorimetry, or the heat-pulse method (HPM). It is based on the principle $C(T) \equiv \lim_{\Delta T \to 0} \frac{\Delta Q(T)}{\Delta T}$ meaning that the heat capacity C of the sample is determined by the pulse heat ΔQ supplied to the sample and the corresponding temperature rise ΔT. The main disadvantages of the method are especially the limitations on both sample size and temperature range. It is not well suited for measurements of small samples at low temperatures because the necessary heat pulse is relatively small under these conditions and heat leaks caused by electrical wiring are therefore causing inaccuracies [16].

The calorimeter we use consists of a vacuum cell, see Figure 2.1, sealed with an indium wire. The cell is then fixed on a tube assembly connecting it to the measuring devices and a diffusion and a rotary vane pump. Maintaining high

vacuum in the cell (after the cooling process) is very important, otherwise the measurement process is not sufficiently adiabatic. Further information about the calorimeters used for this study can be found in Ref. [17, 18].

The cryostat is filled with liquid ^{4}He and afterwards cooled down to the temperature of approximately 1.5 K using the rotary vane pump. The sample is fixed to the sapphire holder with a small amount of vacuum grease Apiezon N.

Heat capacity of the solid solution $CeCo_xRh_{1-x}Si_3$ was measured using the same method, the measurements were carried out at the Joint Laboratory for Magnetic Studies of Department of Condensed Matter Physics of Charles University [19] using a Physical Property Measurement System with 9 (14) T superconducting coil from Quantum Design [20].

2.4 Electrical Resistivity

The electrical resistivity was measured using one of the most common methods: the 4-point method. The measurements of the solid solution $CeIr(Si_xGe_{1-x})_3$ were carried out at the Institute of Solid State Physics at Vienna University of Technology [15] while the measurements of the solid solution $CeCo_xRh_{1-x}Si_3$ were carried out at the Joint Laboratory for Magnetic Studies of Department of Condensed Matter Physics of Charles University [19]. The samples are cut into approximately a shape of a square cuboid and afterwards contacted with 4 wires arranged linearly along the longest dimension of the sample. The two outer probes are used later on to carry electric current into the sample while the inner two probes are used for the measurement of the induced voltage. The main advantage of this technique is elimination of inaccuracies caused by resistance of the contacts and the wiring and thermovoltages, when using an AC mode.

While known electrical current I is applied on the outer probes the potential difference U between the inner probes is measured. Using Ohms's law

$$I = \frac{U}{R} \tag{2.1}$$

we obtain the resistance R of the sample. The resistivity ρ is afterwards calculated from the formula

$$\rho = R\frac{A}{l}, \tag{2.2}$$

where l is the length of the sample and A cross-sectional area of the sample.

In the present measurements, gold wires with a diameter of 25 μm are used, the samples are glued to the holder with the insulating GE Varnish and the gold wire contacs are fixed using the silver-filled epoxy system *EPO-TEK ®H20E* [21].

The measurement itself is then carried out in a cryostat filled with liquid ^{4}He. After the desired low temperature is reached the measurement is started, making use of the temperature drift towards the room temperature.

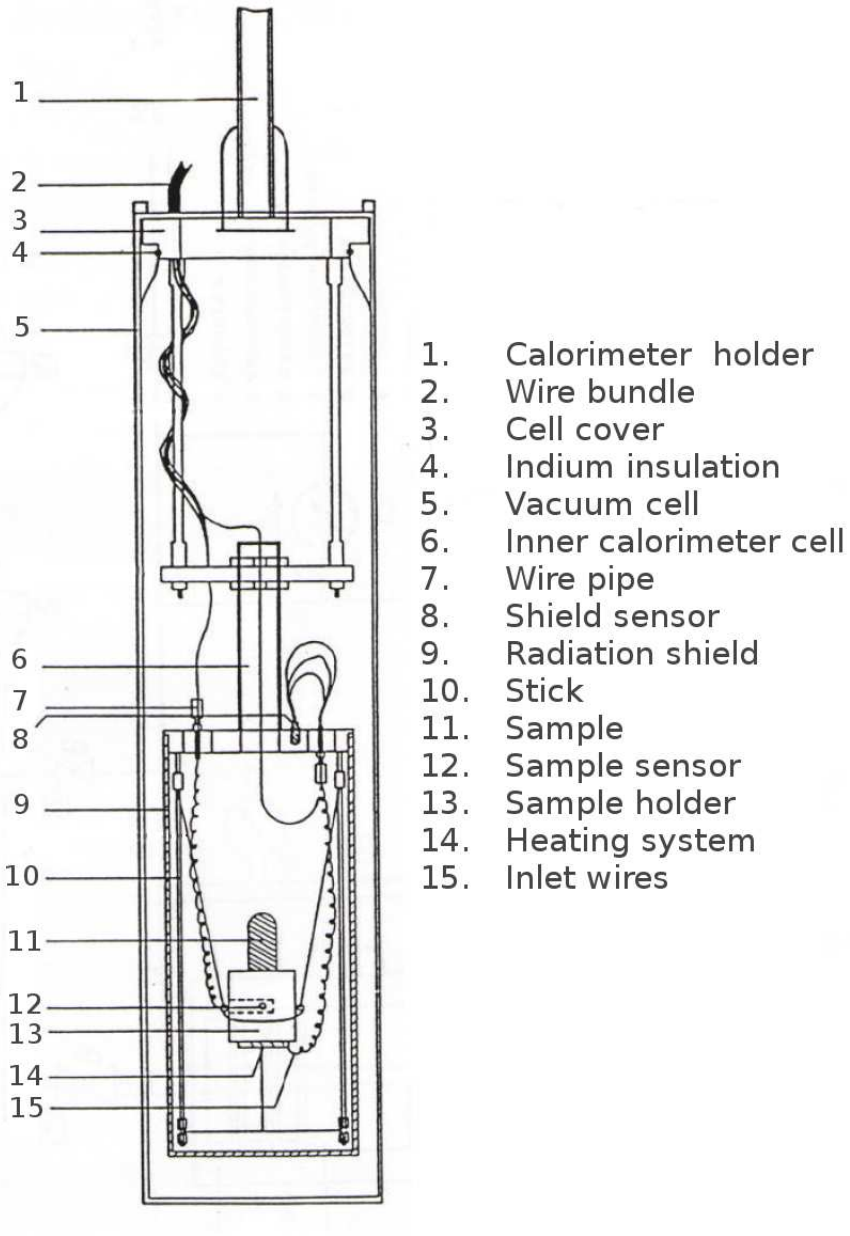

Figure 2.1: Schema of the calorimeter vacuum cell

2.5 Magnetic Properties

2.5.1 SQUID

The Superconducting QUantum Interference Device (SQUID) combines the physical phenomena of flux quantization and Josephson tunneling.

In SQUID it is possible to detect a change in applied magnetic flux corresponding to a tiny fraction of one flux quantum, typically 10^{-6} ϕ_0 $\mathrm{Hz}^{-1/2}$ in today's devices. SQUIDs – which are intrinsically flux-to-voltage transducers – are the most sensitive detectors of magnetic flux known [22].

Our measurements were carried out using a Cryogenic S600X SQUID magnetometer at the Institute of Solid State Physics at Vienna University of Technology [15].

3. Results – $CeCo_xRh_{1-x}Si_3$

3.1 X-ray Diffraction

The X-ray Diffraction measurements were carried out as described in Section 2.2. The results of the measurements reveal a linear variation of the unit cell volume, the asymptotic standard error of the linear fit is smaller than 7 %. The unit cell parameters a and c obtained within this study are summarized in Table 3.1 and plotted in Figure 3.1.

Composition	a [pm]	c [pm]
$CeCo_{0.5}Rh_{0.5}Si_3$	(418.82 ± 0.06)	(968.2 ± 0.3)
$CeCo_{0.8}Rh_{0.2}Si_3$	(416.11 ± 0.04)	(961.7 ± 0.2)
$CeCo_{0.9}Rh_{0.1}Si_3$	(414.88 ± 0.03)	(959.6 ± 0.1)
$CeCoSi_3$	(413.44 ± 0.02)	(956.61 ± 0.08)

Table 3.1: Lattice parameters of $CeCo_xRh_{1-x}Si_3$ determined with X-ray diffraction measurements.

3.2 Specific Heat

The specific heat of the samples was measured using a heat-pulse calorimeter, see Section 2.3. The masses of the examined samples of $CeCo_xRh_{1-x}Si_3$, $x = 0.5$, $x = 0.8$, $x = 0.9$ and $x = 1.0$ were 5.82 mg, 5.83 mg, 5.85 mg and 4.60 mg, respectively. In the region below 1.8 K the specific heat of all four samples exhibits just a small bump but not a clear superconducting phase transition. We therefore display only the specific heat of $CeCo_{0.8}Rh_{0.2}Si_3$ as an illustration of the specific heat of the studied solid solution, see Figure 3.2.

3.3 Electrical Resistivity

The electrical resistivity of the samples was measured using the 4-point method, see Section 2.4. The temperature and field dependence of the relative electrical resistivity is plotted in Figures 3.3 and 3.4. The temperature dependence in a non-zero magnetic field does not exhibit any interesting behaviour, we thus present only the results for $CeCo_{0.5}Rh_{0.5}Si_3$ as an illustration. In order to smooth out the short-term fluctuations a running average is displayed for $CeCoSi_3$.

The electrical resistivity of the samples exhibits a superconducting phase transition at 0.7–0.9 K which is consistent with the previous results reported in Ref. [5] for $CeCoSi_3$. The transition slightly shifts towards lower temeperatures in the Co richer compositions. The magnetic field dependence of the resistivity shows a suppression of superconductivity in fields above 12–15 mT.

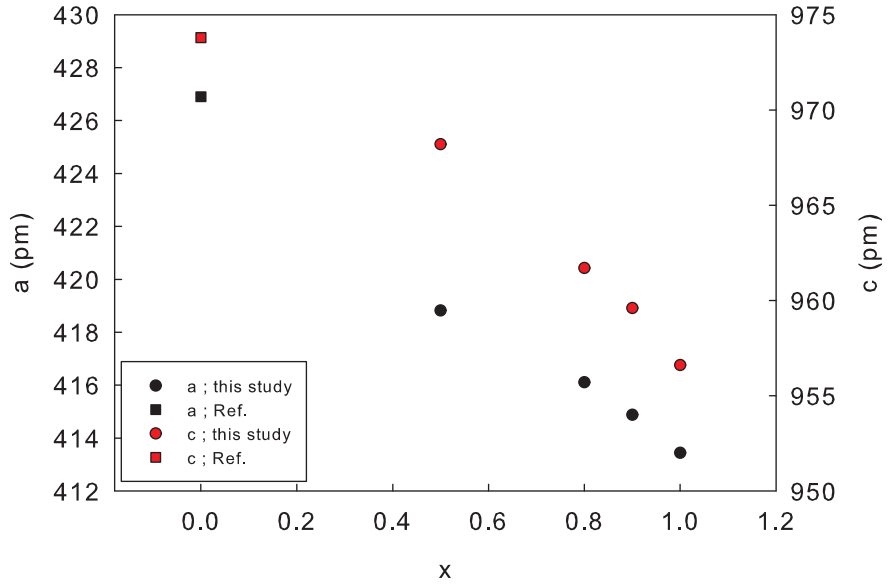

Figure 3.1: Lattice parameters of $CeCo_xRh_{1-x}Si_3$. The value for $x = 0$ is taken from Ref. [7].

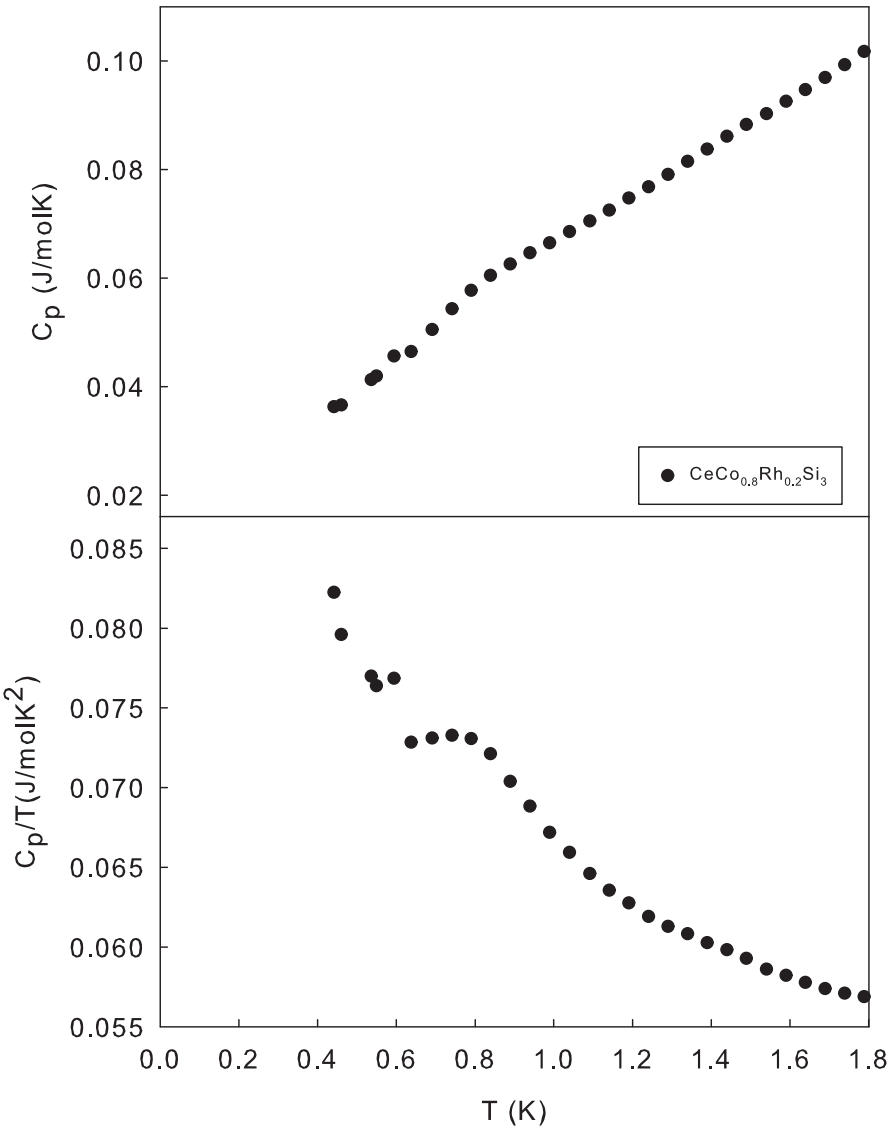

Figure 3.2: Illustration of specific heat of $CeCo_xRh_{1-x}Si_3$ in a plot C_p vs T and C_p/T vs T.

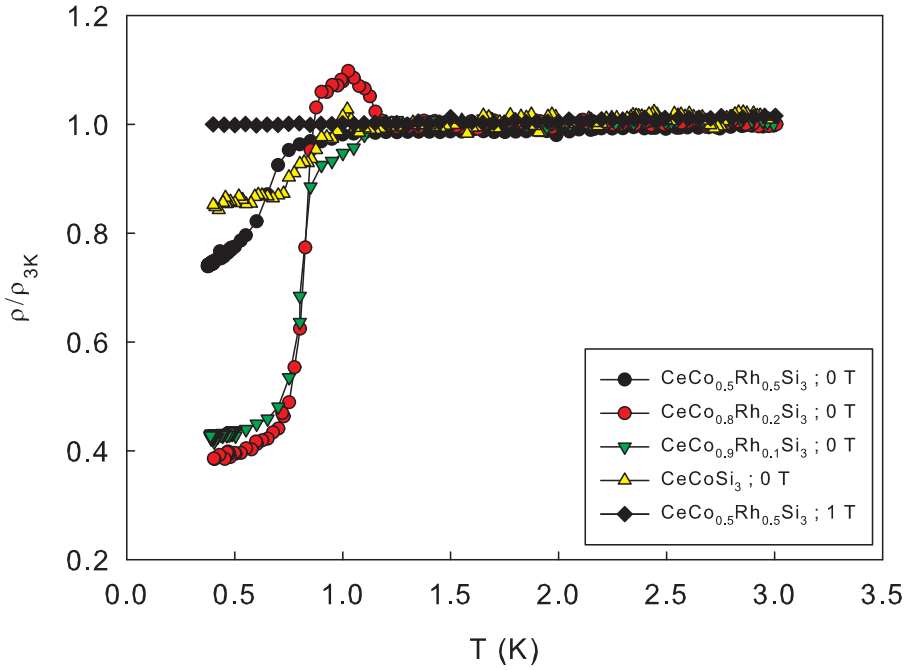

Figure 3.3: Temperature dependence of the relative electrical resistivity of $CeCo_xRh_{1-x}Si_3$ in a zero magnetic field and an illustration of the temperature dependence in a non-zero magnetic field.

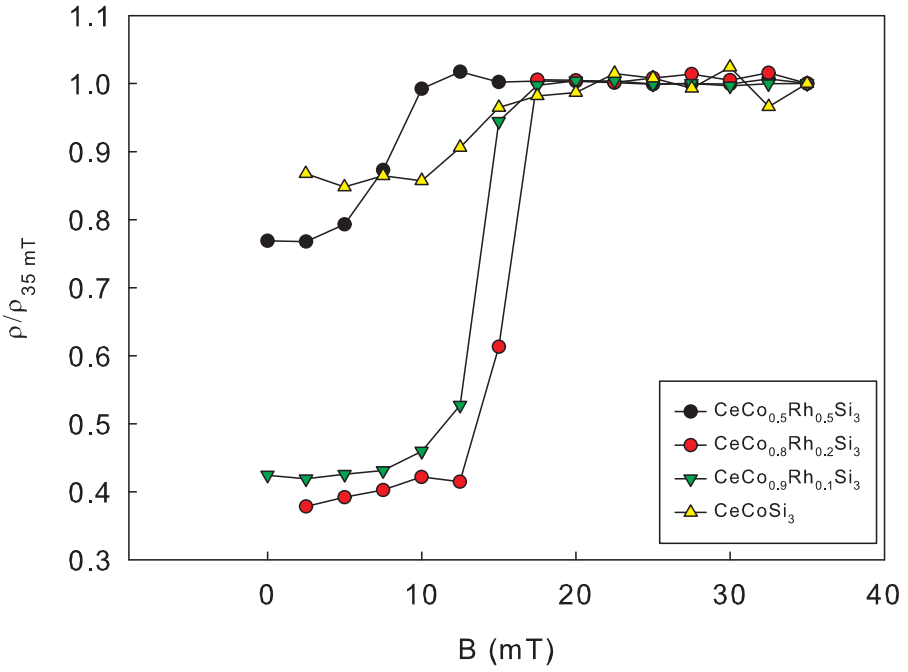

Figure 3.4: Magnetic field dependence of the relative electrical resistivity of $CeCo_xRh_{1-x}Si_3$ at 400 mK.

4. Results – $CeIr(Si_xGe_{1-x})_3$

4.1 X-ray Diffraction

The X-ray Diffraction measurements were carried out as described in Section 2.2. The results of the measurements reveal a linear variation of the unit cell volume, the asymptotic standard error of the linear fit is smaller than 16 %. The results, the unit cell parameters a and c, are summarized in Table 4.1. The parameters are also plotted in Figure 4.1 including lattice parameters of some further substitutions provided for comparison by J. Prokleška.

Composition	a [pm]	c [pm]
$CeIr(Si_{0.1}Ge_{0.9})_3$	(438.52 ± 0.04)	(998.8 ± 0.1)
$CeIr(Si_{0.4}Ge_{0.6})_3$	(434.35 ± 0.04)	(994.3 ± 0.2)
$CeIr(Si_{0.6}Ge_{0.4})_3$	(431.20 ± 0.04)	(990.4 ± 0.1)
$CeIr(Si_{0.8}Ge_{0.2})_3$	(426.89 ± 0.04)	(983.4 ± 0.1)

Table 4.1: Lattice parameters of $CeIr(Si_xGe_{1-x})_3$ determined with X-ray diffraction measurements.

4.2 Specific Heat

The specific heat of the samples was measured using a heat-pulse calorimeter, see Section 2.3. The masses of the examined samples of $x = 0.1$, $x = 0.4$, $x = 0.6$ and $x = 0.8$ were 1.66131 g, 1.0068 g, 1.66863 g and 1.51724 g, respectively. The results of all the solid solutions in field 0 T are plotted in Figure 4.2 and separately – also in non-zero magnetic fields – in Figures 4.4, 4.5, 4.6 and 4.7.

Generally, the Ge richer compositions exhibit more phase transitions. The specific heat of $CeIr(Si_{0.1}Ge_{0.9})_3$ exhibits a step like anomaly at $T_N = 8.4$ K, suggesting a second order phase transition, a weak bump at $T_1^* = 6.9$ K and a sharp peak like anomaly at $T_2^* = 4.9$ K. The composition $CeIr(Si_{0.4}Ge_{0.6})_3$ exhibits three anomalies as well. The specific heat suggests a second order phase transition at $T_N = 7.9$ K and a phase transition at $T_2^* = 5.1$ K. A weak jump like anomaly is observed at the temperature of $T_1^* = 6.9$ K as well. Specific heat of $CeIr(Si_{0.6}Ge_{0.4})_3$ reveals only one peak like anomaly at $T_N = 6.4$ K suggesting a first order phase transition. The specific heat of $CeIr(Si_{0.8}Ge_{0.2})_3$ exhibits a peak like anomaly at $T_N = 4.2$ K, also suggesting a first order phase transition.

For two samples, specific heat in a non-zero magnetic field was measured as well. For the solid solution $CeIr(Si_{0.4}Ge_{0.6})_3$, displayed in Figure 4.5, the peak which signals the magnetic phase transition at $T_2^* = 5.1$ K is suppressed when magnetic field is applied whereas the antiferromagnetic step at $T_N = 7.9$ K exhibits quite the opposite behaviour. With the solid solution $CeIr(Si_{0.8}Ge_{0.2})_3$, Figure 4.7, no significant changes in the height of the peak at $T_{N2} = 4.2$ K are observed, when magnetic field is applied, only its position seems to be slightly

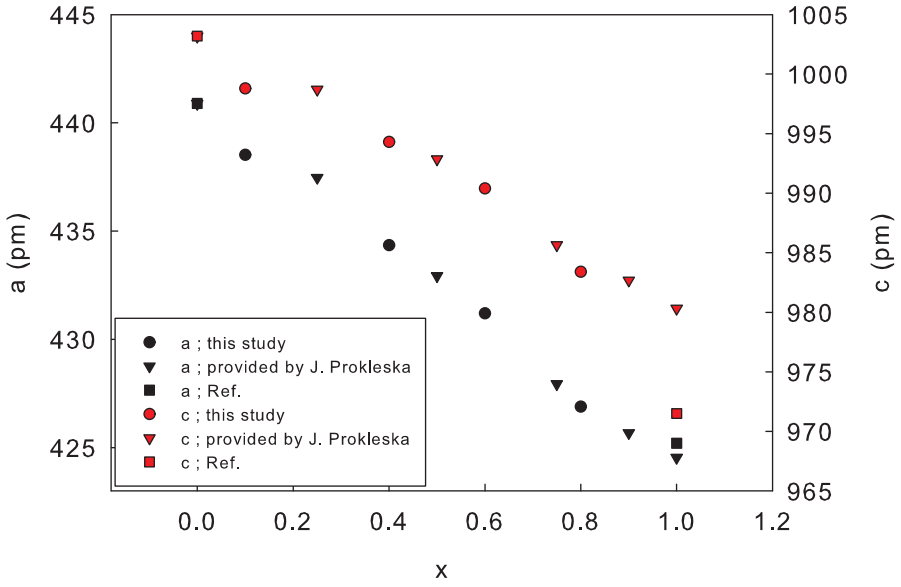

Figure 4.1: Lattice parameters of $CeIr(Si_xGe_{1-x})_3$ obtained within this study, provided by J. Prokleška and from Ref. [7].

shifted towards lower temperatures, suggesting a robust antiferromagnetic order. A small anomaly at $T^* = 7.5$ K is also observed when applying a magnetic field of 3 T.

4.3 Electrical Resistivity

The length l of the samples was measured using a microscope equipped with a reticle, the remaining two dimensions a and b are measured with Vernier caliper. Dimensions of the measured samples are listed in Table 4.2.

Sample	a [mm]	b [mm]	l [mm]
$CeIr(Si_{0.1}Ge_{0.9})_3$	1.00	0.75	3.3
$CeIr(Si_{0.4}Ge_{0.6})_3$	0.72	0.68	1.4
$CeIr(Si_{0.6}Ge_{0.4})_3$	0.51	0.36	1.4
$CeIr(Si_{0.8}Ge_{0.2})_3$	0.95	0.55	1.8

Table 4.2: Dimensions of the samples used for resistivity measurements.

The electrical resistivity of the samples was then measured using the 4-point method, see Section 2.4.

The results have revealed that the absolute value of electrical resistivity of $CeIr(Si_{0.1}Ge_{0.9})_3$ at room temperature exceeds the values of $CeIr(Si_{0.4}Ge_{0.6})_3$ and $CeIr(Si_{0.6}Ge_{0.4})_3$. As this goes directly against the scaling behaviour of the remaining three solid solutions, it is presumed that the absolute values of the electrical resistivity are misleading. This might stem from the fact that the material

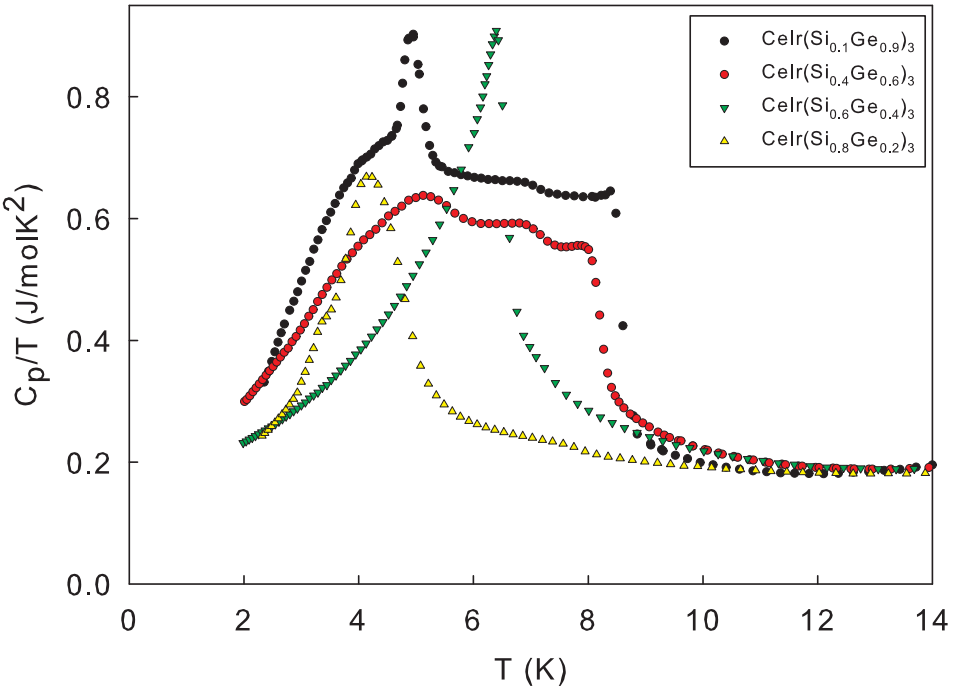

Figure 4.2: Specific heat of $CeIr(Si_xGe_{1-x})_3$ in a plot C_p/T vs T.

contains empty spaces due to the crystallization process and therefore the cross-sectional area of the sample has significant error, typically it is ~ 10–20 %. The electrical resistivity values are thus given relative to the values measured at temperature 292 K.

The results are plotted in Figure 4.3 and including the derivative of the electrical resistivity with respect to temperature in Figures 4.4, 4.5, 4.6 and 4.7.

Both phase transitions at $T_N = 8.4$ K and at $T_2^* = 4.9$ K observed in the specific heat of $CeIr(Si_{0.1}Ge_{0.9})_3$ are also observed in the derivative of its electrical resistivity. The electrical resistivity of $CeIr(Si_{0.4}Ge_{0.6})_3$ exhibits similar dependence as that of $CeIr(Si_{0.1}Ge_{0.9})_3$ with anomalies at different temperatures. The resistivity results however do not confirm the phase transition temperatures established by the specific heat measurements. The resistivity derivatives of $CeIr(Si_{0.6}Ge_{0.4})_3$ and $CeIr(Si_{0.8}Ge_{0.2})_3$ exhibit similar behaviour as their specific heat with peak at approximately the same temperature of $T_N = 6.4$ K and $T_N = 4.2$ K, respectively.

4.4 Magnetic Susceptibility

The magnetic susceptibility is measured using the SQUID magnetometer, see Section 2.5.1, and a Quantum Design PPMS (Physical Property Measurement System). The masses of the samples used for the measurements are collected in Table 4.3.

The results from the SQUID measurements are plotted in Figures 4.4, 4.5, 4.6 and 4.7.

The second order phase transition at $T_N = 8.4$ K of $CeIr(Si_{0.1}Ge_{0.9})_3$ suggested by specific heat and electrical resistivity is not visible in the magnetic susceptibil-

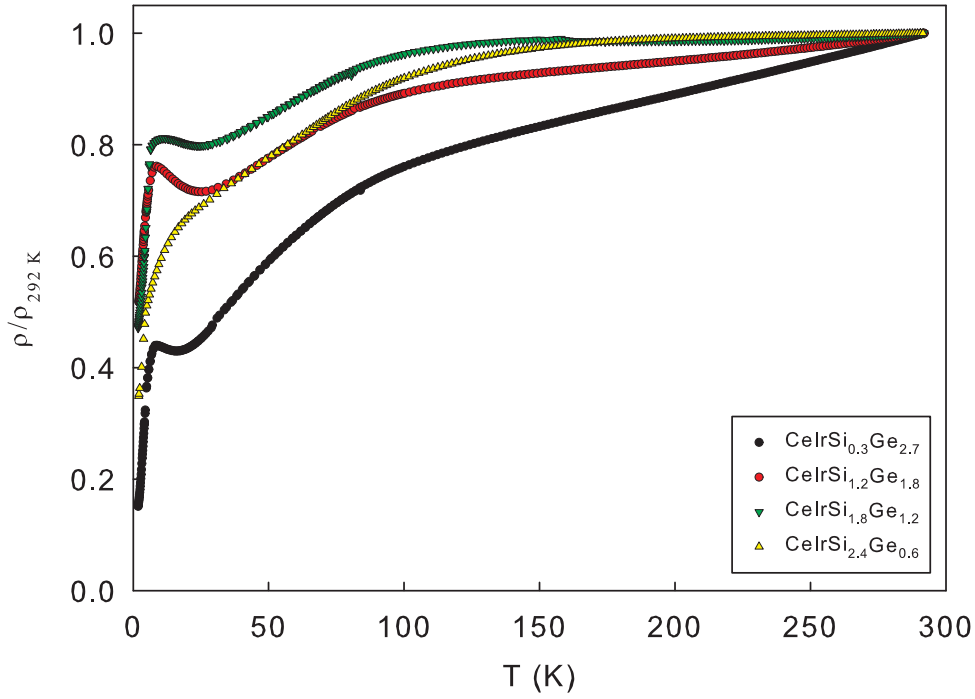

Figure 4.3: Temperature dependence of the relative electrical resistivity of $CeIr(Si_xGe_{1-x})_3$.

ity, see inset in Figure 4.4. The weak jump like anomaly at $T_1^* = 6.9$ K in specific heat on the other hand can be seen in the magnetic susceptibility. The susceptibility exhibits a ferromagnetic behaviour below $T_2^* = 4.9$ K confirming the first order phase transition indicated by the specific heat measurement. The magnetic susceptibility of the composition $CeIr(Si_{0.4}Ge_{0.6})_3$ suggests the same transitions as the specific heat at the temperatures $T_2^* = 5.1$ K and $T_N = 7.9$ K – small but nevertheless significant anomalies are observed. At roughly the ordering temperature $T_N = 6.4$ K the susceptibility of the composition $CeIr(Si_{0.6}Ge_{0.4})_3$ exhibits an anomaly below which an antiferromagnetic dependence is observed, it therefore agrees with the suggestions from the specific heat measurements. The magnetic susceptibility of $CeIr(Si_{0.8}Ge_{0.2})_3$ exhibits an antiferromagnetic behaviour below aproximately 5.3 K, roughly agreeing with the first order phase transition at $T_N = 4.2$ K suggested by the specific heat measurements. Furthermore, the magnetic susceptibility exhibits a ferromagnetic behaviour in temperature from 5.3 K up to aproximately 8.2 K we thus presume that anomaly at $T^* = 7.5$ K observed in specific heat under magnetic field of 3 T is caused by a ferromagnetic impurity.

For the Curie-Weiss fits the data from PPMS are used. Since in the PPMS the samples are fixed with vacuum fat and Teflon tape between two pieces of quartz, the data from SQUID is considered more accurate. However, with the PPMS the measurements are carried out up to the temperature of 400 K (in SQUID only up to room temperature), the paramagnetic fit becomes therefore more meaningful.

Fits of the Curie-Weiss law (Eq. 1.7) in the temperature range of 100–400 K and 250–400 K are carried out. Some of the values of the Pauli susceptibility obtained from fits in the range 100–400 K are significantly exceeding the realistic

Sample	m_{SQUID} [mg]	m_{PPMS} [mg]
$CeIr(Si_{0.1}Ge_{0.9})_3$	12.26	104.75
$CeIr(Si_{0.4}Ge_{0.6})_3$	19.92	90.73
$CeIr(Si_{0.6}Ge_{0.4})_3$	26.36	153.85
$CeIr(Si_{0.8}Ge_{0.2})_3$	16.30	168.62

Table 4.3: Masses of the samples used for magnetic susceptibility measurements in SQUID and PPMS.

values. The values from the temperature range 250–400 K were thus used. Further on, in this temperature range fits with and without the Pauli susceptibility (with and without the χ_0 in equation 1.7) are carried out. The fits carried out with the function containing also the Pauli susceptibility reveal values which are differing from the values of the other fit only by 0–3 %. Since these deviations are comparable to the precision of the PPMS, the values from fits without the Pauli susceptibility are used. From the coefficients of the fit the effective magnetic moment is calculated, see equation 1.9. The results are summarized in Table 4.4. Figure 4.8 contains the obtained data of the inversed magnetic susceptibility as well as the fitted linear functions.

Sample	C [emu·K/mol]	Θ [K]	μ_{eff} [μ_B]
$CeIr(Si_{0.1}Ge_{0.9})_3$	0.7737	-33.4	2.49
$CeIr(Si_{0.4}Ge_{0.6})_3$	0.7977	-65.0	2.53
$CeIr(Si_{0.6}Ge_{0.4})_3$	0.8023	-68.1	2.53
$CeIr(Si_{0.8}Ge_{0.2})_3$	0.8106	-79.7	2.55

Table 4.4: The Curie-Weiss constant, the Weiss temperature θ and effective magnetic moment values obtained from the PPMS measurement data.

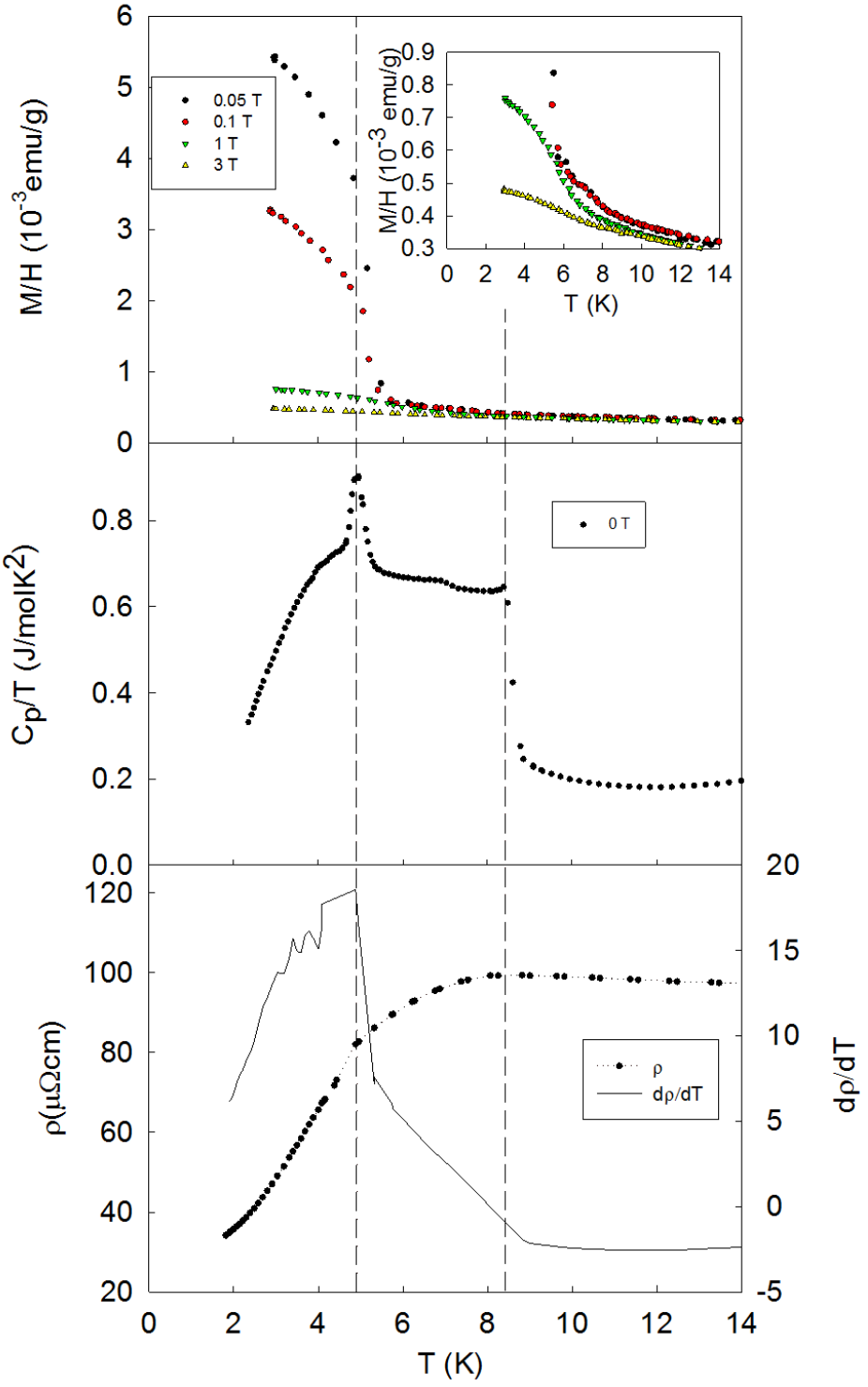

Figure 4.4: The temperature dependence of magnetic susceptibility of $CeIr(Si_{0.1}Ge_{0.9})_3$ in a plot M/H vs T, temperature dependence of specific heat in a plot C_p/T vs T, temperature dependence of electrical resistivity and the temperature derivative of electrical resistivity. The inset displays the dependence of magnetic susceptibility on a different scale.

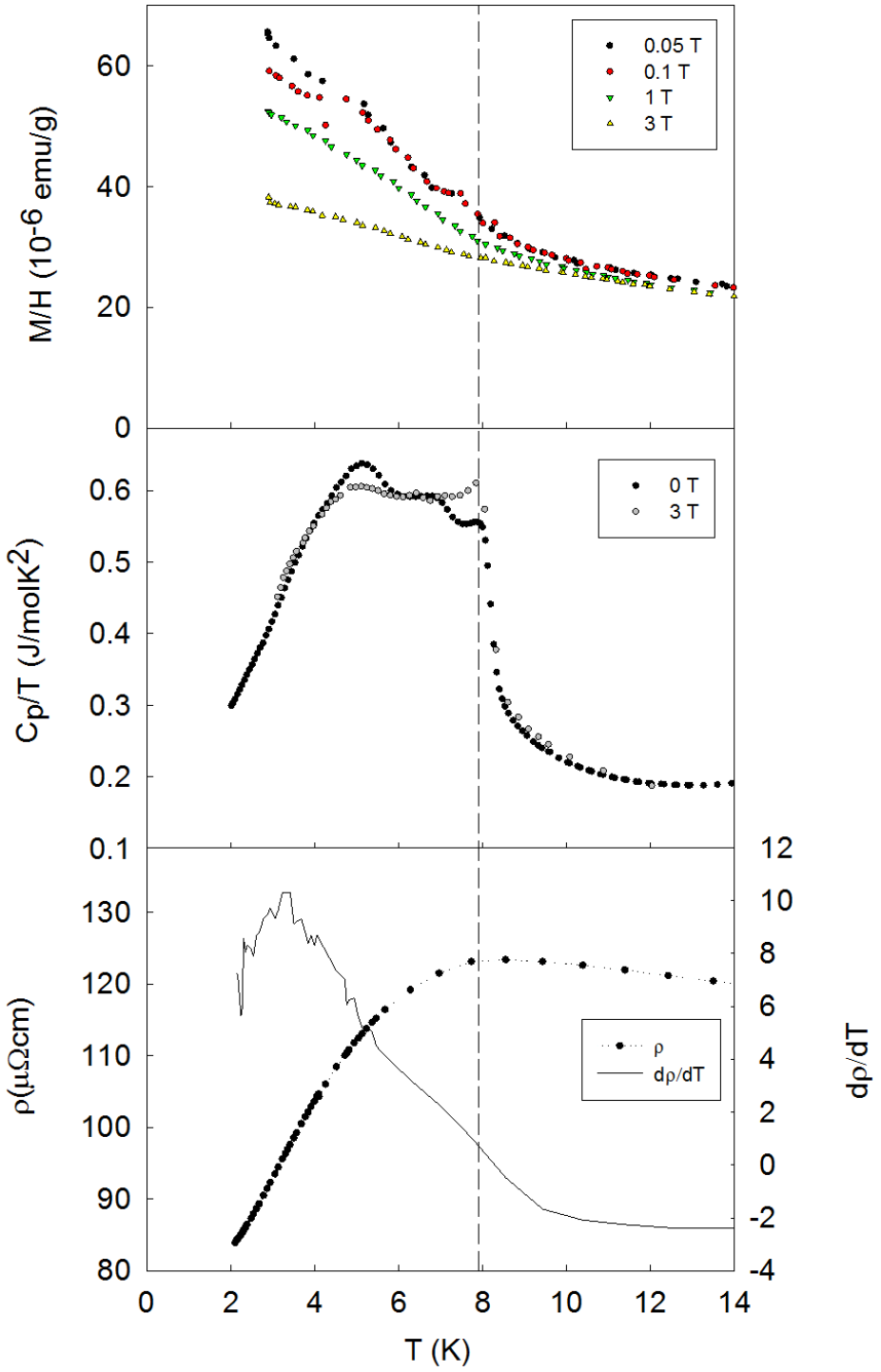

Figure 4.5: The temperature dependence of magnetic susceptibility of $CeIr(Si_{0.4}Ge_{0.6})_3$ in a plot M/H vs T, temperature dependence of specific heat in a plot C_p/T vs T, temperature dependence of electrical resistivity and the temperature derivative of electrical resistivity.

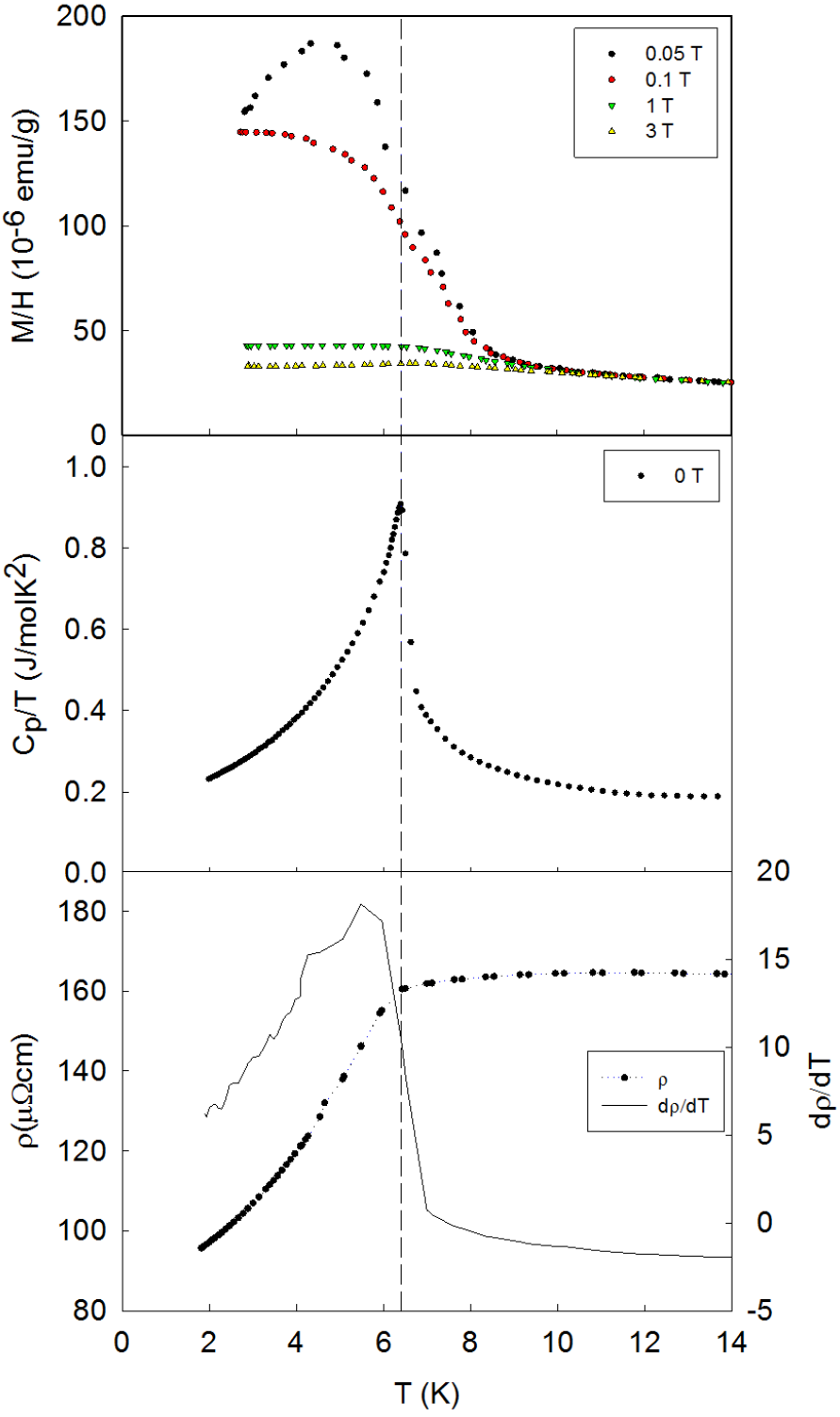

Figure 4.6: The temperature dependence of magnetic susceptibility of $CeIr(Si_{0.6}Ge_{0.4})_3$ in a plot M/H vs T, temperature dependence of specific heat in a plot C_p/T vs T, temperature dependence of electrical resistivity and the temperature derivative of electrical resistivity.

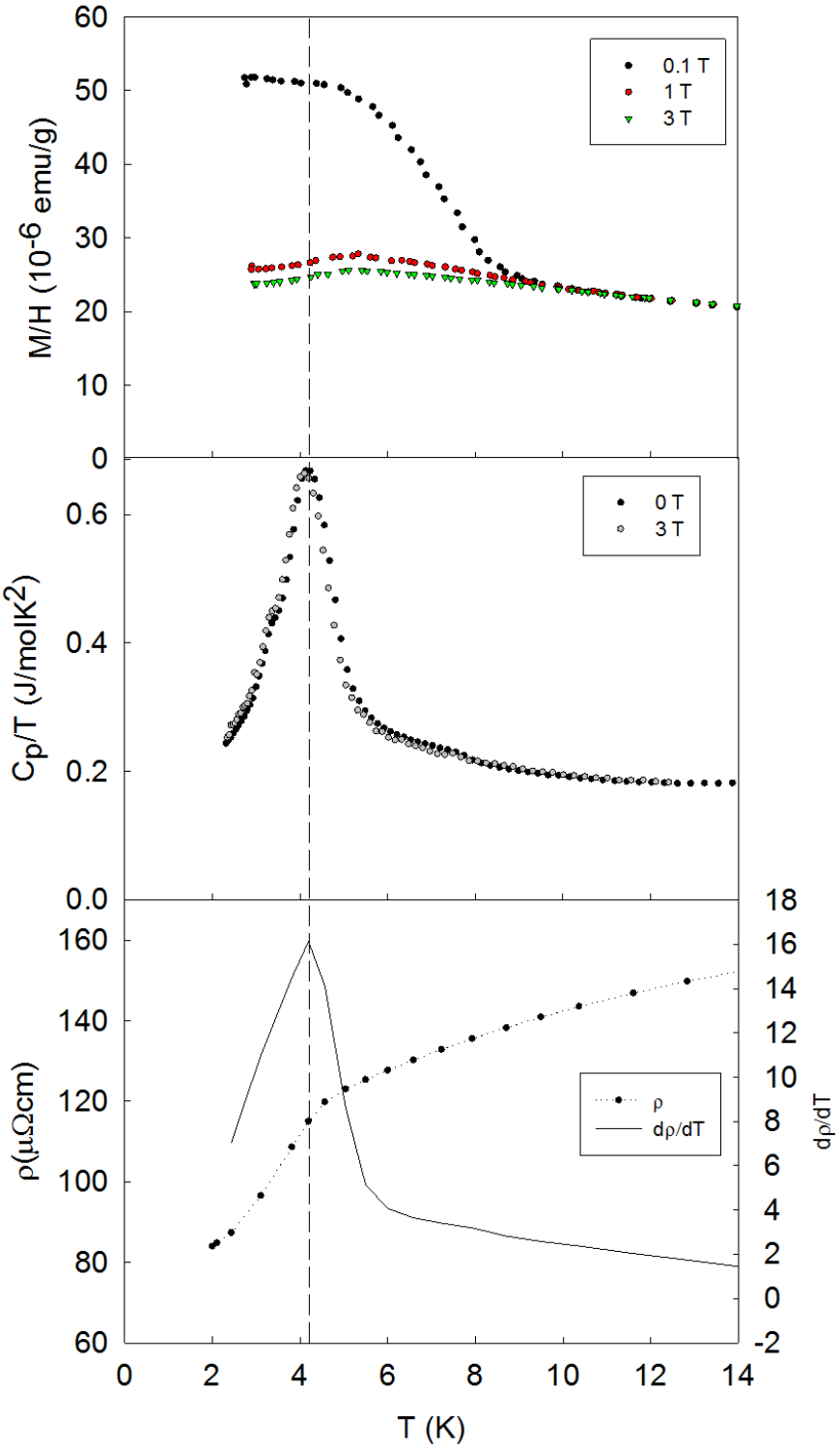

Figure 4.7: The temperature dependence of magnetic susceptibility of $CeIr(Si_{0.8}Ge_{0.2})_3$ in a plot M/H vs T, temperature dependence of specific heat in a plot C_p/T vs T, temperature dependence of electrical resistivity and the temperature derivative of electrical resistivity.

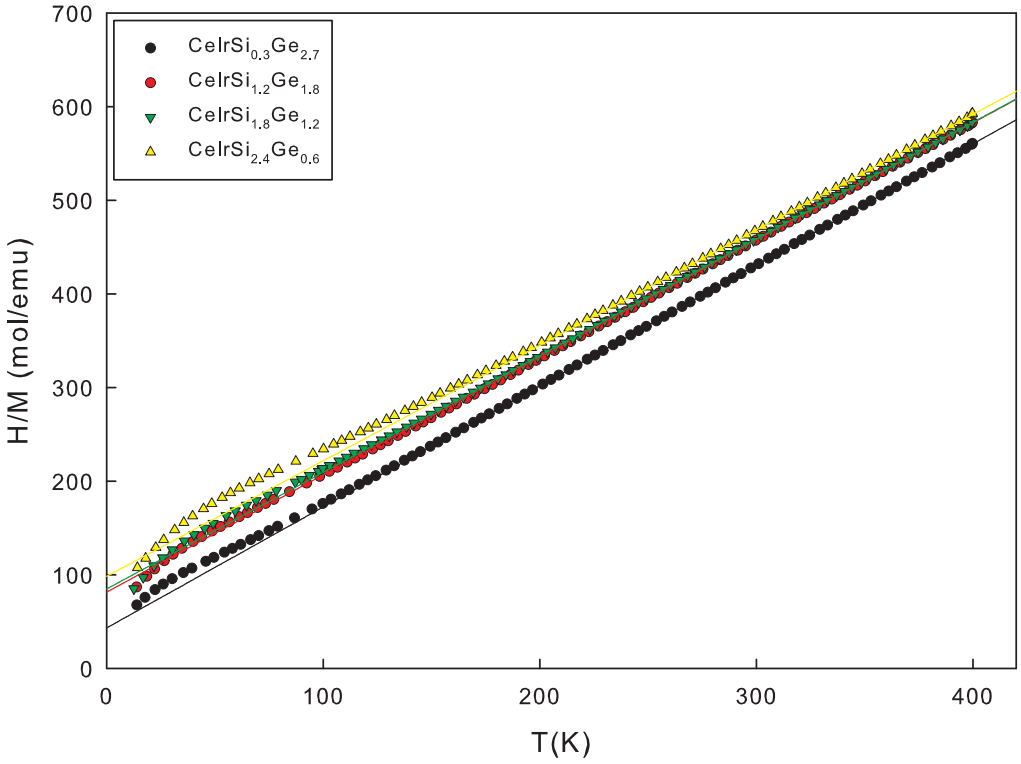

Figure 4.8: The inverse magnetic susceptibility of $CeIr(Si_xGe_{1-x})_3$ in a plot H/M vs T, measured using PPMS. Applied magnetic field was 3T, only every 100^{th} measured point is shown.

5. Discussion

We succeeded in growing the desired polycrystalline samples of the solid solution $CeCo_xRh_{1-x}Si_3$. All of the studied compositions exhibit a superconducting transition at approximately the same temperature of 0.7–0.9 K, see Figure 3.3. The transition is not visible in the specific heat though – all it exhibits is just a small bump, see Figure 3.2. A transition to a superconducting state however is of second order and causes a discontinuity in the specific heat of the sample, see Section 1.3. Thus if the entire sample underwent a transition into the superconduting state the specific heat would exhibit a clear, probably jump like, anomaly which it does not. We therefore conclude that the observed superconductivity is probably caused by certain impurity phases. Our conclusion agrees with the results of an independent study published in Ref. [23]. Since this study was published in the course of our research we decided to focus on the solid solution $CeIr(Si_xGe_{1-x})_3$ instead.

We have prepared four polycrystalline samples of $CeIr(Si_xGe_{1-x})_3$ ($x = 0.1$, $x = 0.4$, $x = 0.6$ and $x = 0.8$) and measured its crystallographic, thermodynamic and magnetic properties. Using a simple numerical integration we calculated an approximate change ΔS in magnetic entropy of the compositions in the region from $T_A = 2.3$ K up to $T_B = 14$ K. Since we want to compare the individual changes of magnetic entropy we also subtracted the $S_0 = (T_B - T_A)k$, where $k = 0.180\ \mathrm{J/molK^2}$ is the minimal value of C_p/T of all four compositions on the interval $(T_A; T_B)$. We therefore subtracted the change in entropy S_0 common to all the compositions. The results are plotted in Figure 5.1, revealing a decreasing, almost linear, dependency. We are curious what is the origin of this behaviour. The compounds might either exhibit another transition at lower temperatures to balance the change in entropy, or the valence of the present Cerium atoms changes.

Based on the measurements of the specific heat, electrical resistivity and magnetic susceptibility we have established the magnetic phase transition temperatures. The established phase transition temperatures T_2^* and T_N in relation to the unit cell volume were plotted into Figure 5.2, making use of Figure 2. The present results are thus in clear contrast with the non-monotonous relation between the Néel temperature and the unit cell volume proposed by Kawai et al. [8], see Figure 5.2. We have therefore tried to find a different and valid scaling between the ordering temperatures and structural parameters.

In Table 5.1 we summarize our results for the solid solution $CeIr(Si_xGe_{1-x})_3$ with the previously published results for the $BaNiSn_3$ type $CeTX_3$ compounds. We display the values of the lattice parameters, shortest interatomic distances Ce-Ce and Ce-T and the Néel temperatures and in Figure 5.3 we plot the Néel temperatures scaled to the various structural parameters. Unfortunately, none of the studied scalings have unraveled a simple Néel temperature dependency valid for all compounds.

The values of the Weiss temperature of the solid solution $CeIr(Si_xGe_{1-x})_3$ summarized in Table 4.4 decrease from -33 K down to -80 K for $x = 0.1 - 0.8$ which is consistent with the Weiss temperature of -21 K for $x = 0$ and -142 K for $x = 1$ measured in Ref. [7]. The effective magnetic moment varies only

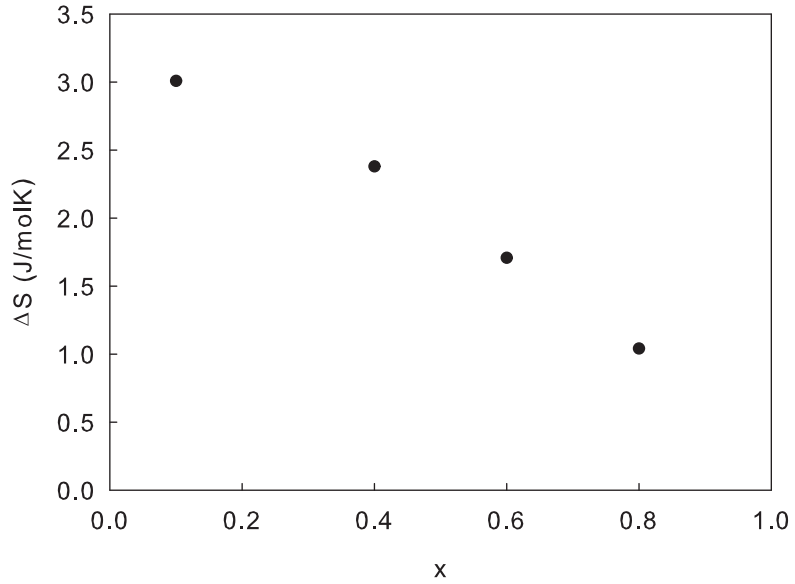

Figure 5.1: Approximate change in magnetic entropy of $CeIr(Si_xGe_{1-x})_3$, as labeled, in a plot ΔS vs x.

Compound	a [pm]	c [pm]	Ce-Ce [pm]	Ce-T [pm]	T_N [K]	
$CeRhSi_3$	423.7	978.5	423.7*	335.9*	1.8	[24, 7]
$CePdSi_3$	433.0	963.1	-	-	5.2	[25]
$CeIrSi_3$	425.2	971.5	425.2	324.9	5	[26, 7]
$CePtSi_3$	432.15	960.75	432.15	337.13	4.8	[27]
$CeCoSi_{0.5}Ge_{2.5}$	429.1	979.3	-	-	12.4	[28]
$CeCoSi_{0.75}Ge_{2.25}$	428.0	975.3	-	-	5.5	[28]
$CeCoSi_{0.9}Ge_{2.1}$	426.9	976.7	-	-	4.0	[28]
$CeIr(Si_{0.1}Ge_{0.9})_3$	438.52	998.8	438.52	341.03	8.5	this study
$CeIr(Si_{0.4}Ge_{0.6})_3$	434.35	994.3	434.35	339.47	7.9	this study
$CeIr(Si_{0.6}Ge_{0.4})_3$	431.20	990.4	431.20	338.16	6.4	this study
$CeIr(Si_{0.8}Ge_{0.2})_3$	426.89	983.4	426.90	335.77	4.2	this study
$CeCoGe_3$	432	983.5	431.92	328.71	21.2	[29]
$CeRhGe_3$	439.76	1003.22	439.76	342.3	14.6	[8, 7]
$CeIrGe_3$	440.1	1002.4	440.10	341.71	8.7	[8]

Table 5.1: Lattice parameters a and c, the shortest interatomic distances Ce-Ce and Ce-T and the Néel temperatures T_N of the $BaNiSn_3$ type $CeTX_3$ compounds. *In the Reference the atomic coordinates were assumed to be the same as those in $LaIrSi_3$.

slightly from 2.49 μ_B up to 2.55 μ_B and is also within the range demarcated by the moment 2.39 μ_B for $x = 0$ and 2.62 μ_B for $x = 1$ [7].

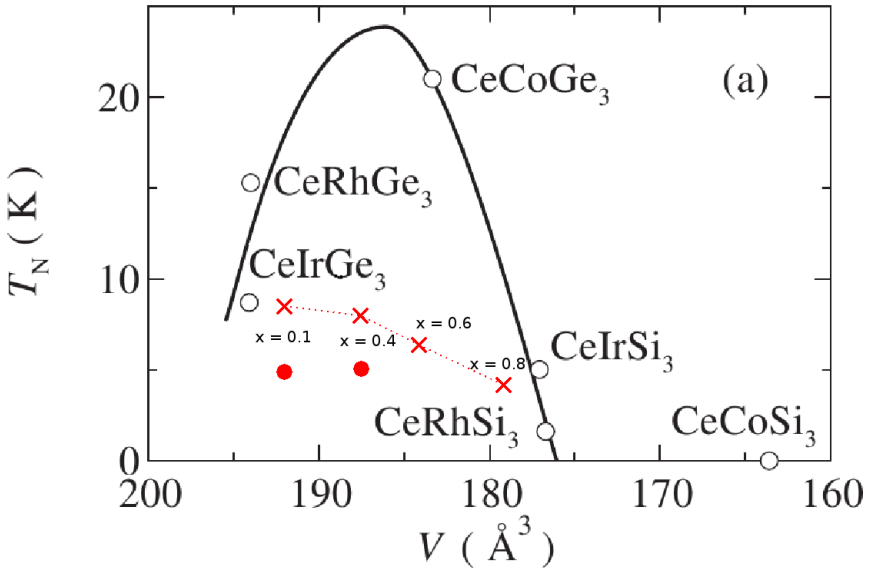

Figure 5.2: Unit cell volume dependence of the Néel temperature in $CeTSi_3$ and $CeTGe_3$ (T: Co, Rh, Ir), reprinted from Ref. [8], with the results from our mesurements of $CeIr(Si_xGe_{1-x})_3$, T_N plotted as diagonal stars and T_2^* plotted as full circles.

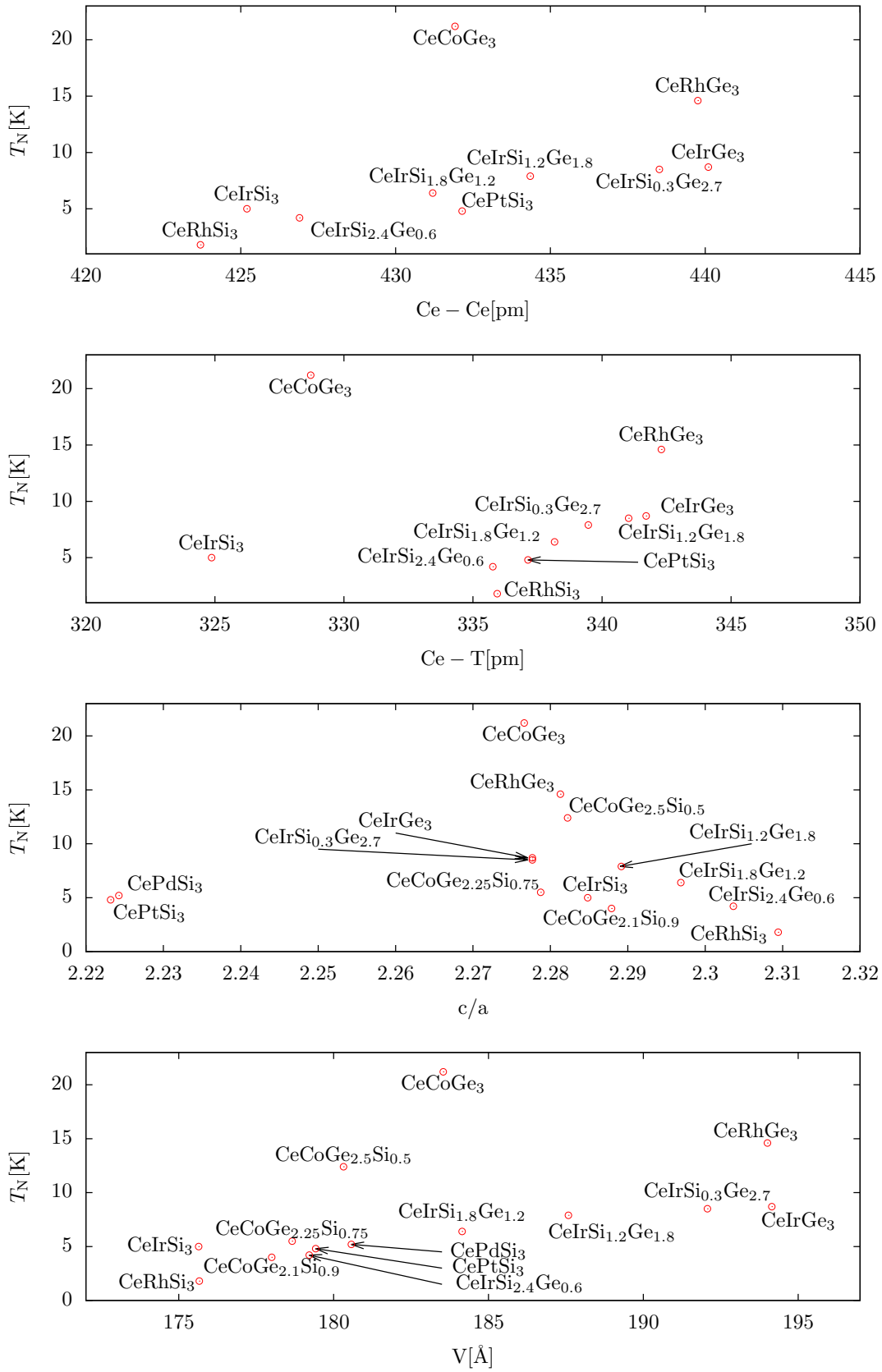

Figure 5.3: The Néel temperature of the $BaNiSn_3$ type $CeTX_3$ compounds in plots T_N vs Ce-Ce, T_N vs Ce-T, T_N vs c/a and T_N vs unit-cell volume V.

Conclusion and Outlook

We have prepared polycrystalline samples of the solid solution $CeCo_xRh_{1-x}Si_3$ ($x = 0.5$, $x = 0.8$, $x = 0.9$ and $x = 1.0$). The superconducting transition at 0.7–0.9 K was observed in all four compositions. Based on the measurements of the specific heat we conclude that the superconductivity is probably caused by impurity phases. Our conclusion is in accordance with results published by M. Smidman et al. [23]. Further focus might be put on preparation of monocrystalline samples of the solid solution in order to supress those impurity phases which occur on the grain boundaries.

All four desired substitutions of the solid solution $CeIr(Si_xGe_{1-x})_3$ ($x = 0.1$, $x = 0.4$, $x = 0.6$ and $x = 0.8$) exist and we have managed to grow polycrystalline samples. Based on various measurements we have determined the crystallographic, thermodynamic and magnetic properties of the solid solution. An estimation of the change of (mainly) magnetic entropy has been established, revealing a decreasing, almost linear, dependency with respect to x. It would be interesting to study the critical temperature and the critical pressure of the supposed pressure-induced superconductivity of the solid solution and their correlation with the change in magnetic entropy. Magnetic phase transition temperatures in relation to x were established. They do not vary significantly but the character of the transitions does. Making use of previously published results, we also tried to find a simple scaling of the Néel temperature of the $BaNiSn_3$ type $CeTX_3$ compounds with respect to basic structural parameters but were not able to establish any dependency valid for all compounds of the group.

Bibliography

[1] N. Kimura and I. Bonalde, "Non-Centrosymmetric Heavy-Fermion Superconductors," in *"Non-Centrosymmetric Superconductors: Introduction and Overview", Lecture Notes in Physics 847*, pp. 35–79, Jan. 2012.

[2] N. Kimura, K. Ito, K. Saitoh, Y. Umeda, H. Aoki, and T. Terashima, "Pressure-Induced Superconductivity in Noncentrosymmetric Heavy-Fermion $CeRhSi_3$," *Physical Review Letters*, vol. 95, p. 247004, Dec. 2005.

[3] I. Sugitani, Y. Okuda, H. Shishido, T. Yamada, A. Thamizhavel, E. Yamamoto, T. D. Matsuda, Y. Haga, T. Takeuchi, R. Settai, and Y. Onuki, "Pressure-Induced Heavy-Fermion Superconductivity in Antiferromagnet $CeIrSi_3$ without Inversion Symmetry," *Journal of the Physical Society of Japan*, vol. 75, p. 043703, Apr. 2006.

[4] F. Honda, I. Bonalde, K. Shimizu, S. Yoshiuchi, Y. Hirose, T. Nakamura, R. Settai, and Y. Onuki, "Pressure-induced superconductivity and large upper critical field in the noncentrosymmetric antiferromagnet $CeIrGe_3$," *Physical Review B*, vol. 81, p. 140507, Apr. 2010.

[5] Y. Iwamoto, K. Ueda, and T. Kohara, "NMR study of $CeCoSi_3$," *Physica B*, vol. 206 & 207, pp. 276–278, 1995.

[6] T. Shimoda, Y. Okuda, Y. Takeda, Y. Ida, Y. Miyauchi, T. Kawai, T. Fujie, I. Sugitani, A. Thamizhavel, T. Matsuda, Y. Haga, T. Takeuchi, M. Nakashima, R. Settai, and Y. Onuki, "Magnetic and electronic properties in $CeTSi_3$ and $CeTGe_3$ (T: transition metal)," *Journal of Magnetism and Magnetic Materials*, vol. 310, pp. 308–309, Mar. 2007.

[7] Y. Muro, D. Eom, N. Takeda, and M. Ishikawa, "Contrasting Kondo-Lattice Behavior in $CeTSi_3$ and $CeTGe_3$ (T=Rh and Ir)," *Journal of the Physical Society of Japan*, vol. 67, no. 10, pp. 3601–3604, 1998.

[8] T. Kawai, H. Muranaka, M.-A. Measson, T. Shimoda, Y. Doi, T. D. Matsuda, Y. Haga, G. Knebel, G. Lapertot, D. Aoki, J. Flouquet, T. Takeuchi, R. Settai, and Y. Onuki, "Magnetic and Superconducting Properties of $CeTX_3$ (T: Transition Metal and X: Si and Ge) with Non-centrosymmetric Crystal Structure," *Journal of the Physical Society of Japan*, vol. 77, p. 064716, June 2008.

[9] N. W. Ashcroft and N. D. Mermin, *Solid State Physics*. 1976.

[10] C. Kittel, *Introduction to Solid State Physics, 8th edition*. John Wiley & Sons, Inc, 2005.

[11] K. Huang, *Statistical Mechanics*. John Wiley & Sons, Inc, 1987.

[12] "Technology Lab, Department of Condensed Matter Physics of Charles University." `http://kfkl.cz/techlab/`, April 2013.

[13] "The X-Ray Group, Department of Condensed Matter Physics of Charles University." http://xray.cz/kfkl-osa/eng/osainst.htm, April 2013.

[14] J. Rodriguez-Carvajal, "Recent advances in magnetic structure determination by neutron powder diffraction," *Physica B*, vol. 192, pp. 55–69, 1993.

[15] "Institute of Solid State Physics, Vienna University of Technology." http://www.ifp.tuwien.ac.at, March 2013.

[16] J. S. Hwang, K. J. Lin, and C. Tien, "Measurement of heat capacity by fitting the whole temperature response of a heat-pulse calorimeter," *Review of Scientific Instruments*, vol. 68, no. 1, pp. 94 – 101, 1997.

[17] H. Michor Master's thesis, Institute for Experimental Physics, 1993.

[18] G. Schaudy, *Kalorimetrie in Hohen Magnetfeldern*. PhD thesis, Institute for Experimental Physics, 1995.

[19] "Joint Laboratory for Magnetic Studies, Department of Condensed Matter Physics of Charles University." http://kfkl.cz/jlms/, April 2013.

[20] "Physical Property Measurement System, Quantum Design." http://www.qdusa.com/products/ppms.html, April 2013.

[21] E. T. Inc., "EPO-TEK H20E technical data sheet." http://www.epotek.com/SSCDocs/datasheets/h20e.pdf, March 2013.

[22] J. Clarke and A. I. Braginski, eds., *The SQUID Handbook*. WILEY-VCH Verlag GmbH and Co. KGaA, 2004.

[23] M. Smidman, R. P. Singh, M. R. Lees, D. M. Paul, D. T. Adroja, and G. Balakrishnan, "Is $CeCoSi_3$ a superconductor?," *Journal of Physics: Conference Series*, vol. 012068, no. 391, 2012.

[24] T. Terashima, M. Kimata, S. Uji, T. Sugawara, N. Kimura, H. Aoki, and H. Harima, "Fermi surface in $LaRhSi_3$ and $CeRhSi_3$," *Physical Review B*, vol. 78, p. 205107, Nov. 2008.

[25] J. Kitagawa, Y. Muro, N. Takeda, and M. Ishikawa, "Low-temperature Magnetic Properties of Several Compounds in Ce-Pd-X (X=Si, Ge and Al) Ternary Systems," *Journal of the Physical Society of Japan*, vol. 66, no. 7, pp. 2163–2174, 1997.

[26] T. Jeong, "Ab initio studies on the electronic structure of $CeIrSi_3$," *Solid State Communications*, vol. 150, pp. 337–340, Feb. 2010.

[27] T. Kawai, Y. Okuda, H. Shishido, A. Thamizhavel, T. D. Matsuda, Y. Haga, M. Nakashima, T. Takeuchi, M. Hedo, Y. Uwatoko, R. Settai, and Y. Onuki, "Magnetic and Electrical Properties in $CePtSi_3$ without Inversion Symmetry in the Crystal Structure," *Journal of the Physical Society of Japan*, vol. 76, p. 014710, Jan. 2007.

[28] D. Eom, M. Ishikawa, J. Kitagawa, and N. Takeda, "Suppression of Antiferromagnetism by Kondo Effect and Quantum Critical Behavior in $CeCoGe_{3-x}Si_x$," *Journal of the Physical Society of Japan*, vol. 67, no. 7, pp. 2495–2500, 1998.

[29] V. K. Pecharsky, O.-B. Hyun, and K. A. J. Gschneidner, "Unusual magnetic properties of the heavy-fermion compound $CeCoGe_3$," *Physical Review B*, vol. 47, no. 18, 1993.

List of Tables